Journal of Alloys and Compounds 969 (2023) 172467

Contents lists available at ScienceDirect

Journal of Alloys and Compounds

journal homepage: www.elsevier.com/locate/jalcom

Nanostructured-microfibrillar polypyrrole coated NiTi current collectors for high power and shape memory $LiFePO_4$ cathodes for Li-ion batteries

Morteza Torabi [a], S.K. Sadrnezhaad [b,*]

[a] Renewable Energy Department, Niroo Research Institute, Tehran, Iran
[b] Department of Materials Science and Engineering, Sharif University of Technology, P.O. Box 11365–9466, Tehran, Iran

ARTICLE INFO

Keywords:
Li-ion batteries
Olivine cathode
Shape memory alloy
Polypyrrole
Conducting polymer

ABSTRACT

Powering the shape-memory alloy-based actuators and wearables needs flexible and compatible energy sources. Lithium iron phosphates are also attractive for their unique properties for safe operation. This study used NiTi thin film as the shape memory current collector coated with one-dimensional (1D) polypyrrole microfibrils for flexible and high-power lithium-ion batteries. The PPy microfibrils facilitated the electron pathway and improved the rate capability of the $LiFePO_4$ cathode significantly. While the pure LiFePO4 showed a 108 mAh/g capacity at 0.1 C, the nanocomposite with microfibril PPy had 136 mAh/g. Discharging at 10 C was associated with a significant loss of capacity for pure cathode (15 mAh/g), whereas 75 mAh/g for nanocomposite with PPy. The rate capability of the LiFePO4 cathode was also improved significantly using PPy microfibrils. For a single-layer pouch battery, the capacity of the flat cell was retained at about 20 mAh. In contrast, the capacity of the nanocomposite decreased to about 18 mAh after curving the cell and recovered to about 19 mAh once relieving at 1 C.

1. Introduction

Since Goodenough and coworkers introduced LiFePO4 in 1997 [1], it is still the most exciting material among all types of polyanion cathodes due to its electrochemical, environmental, safety, and cost advantages. Due to the low rate capability of the LiFePO4, some strategies were employed to improve this drawback. These improvements are based on: 1. Increasing electron transport in bulk [2] and at the particle surface [3–5]; 2. Modifying the ion transport by using nano-sized LiFePO4 to reduce the Li+ ion diffusion length [6,7] and 3. Facilitating of the ion transport along the surface [8]. All of these improvements significantly affect the olivine's electrochemical performance and rate capability. Goodenough improved the rate performance of the LiFePO4 by using polypyrrole with different strategies [9]. They made a relatively porous cathode with physical binding of LiFePO4 to PPy during electropolymerization of the pyrrole. The porosity helps the electrolyte to diffuse into the cathode particles, and PPy removes the need for carbon black and binder.

Furthermore, the PPy could participate in the Li+ ion intercalation process, yielding higher capacity. It was also shown that the electropolymerized PPy composites perform better than the chemically synthesized PPy-active material electrodes [10]. There are some reports about boosting the LiFePO4 cathode by PPy [11–16] using chemical oxidation by FeCl3 as the oxidizing agent, which needs more steps for making the PPy and preparation of the slurry for coating the substrate. On the other hand, they are designed based on the inflexible conventional lithium-ion batteries, which is not a proper choice for new smart devices.

New materials and devices have recently been developed concurrently with the artificial intelligence (AI) boom. The new intelligent electronic devices need wireless connections, high flexibility and safety, and energy harvesting modules [17,18]. Regarding the performance and safety of lithium-ion batteries, sensing and predicting the battery state of health (SOH) has been discussed in detail using data-driven algorithms [19,20].

In this study, we applied a new approach for making $LiFePO_4$/PPy composites using shape memory NiTi for potential application in flexible devices. Thanks to the diversity of PPy shapes and knowing that the electropolymerization of Py in the presence of the nanoparticles led to 3D growth and compact morphology of the final film [21], we electrodeposited the highly-porous and microfibrillar PPy onto a NiTi thin film as a current collector for high power $LiFePO_4$ cathode for flexible li-ion

* Corresponding author.
E-mail address: sadrnezh@sharif.edu (S.K. Sadrnezhaad).

https://doi.org/10.1016/j.jallcom.2023.172467
Received 15 June 2023; Received in revised form 4 October 2023; Accepted 8 October 2023
Available online 10 October 2023

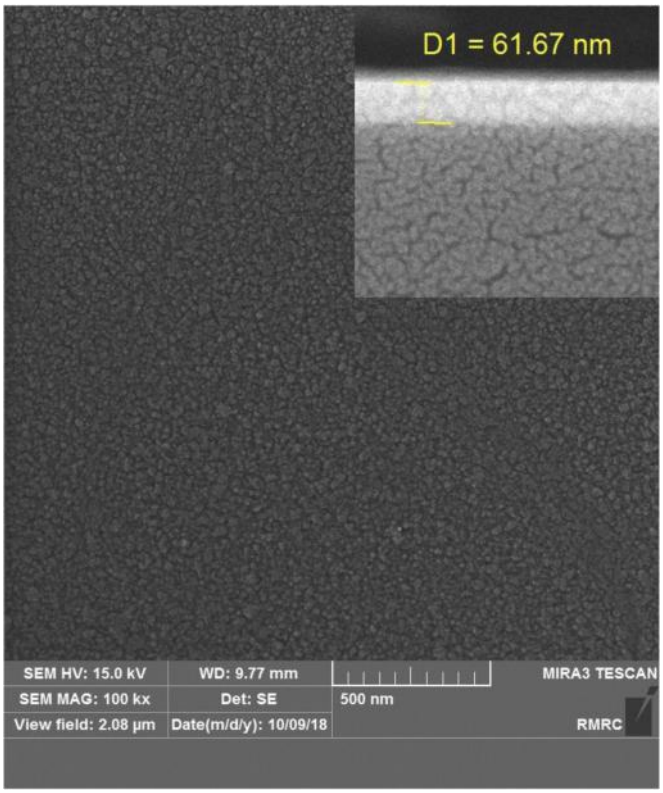

Fig. 1. SEM images of the NiTi thin film coated on the flexible glass (inset: the cross-section of the coated sample).

batteries. The porosity dimension is matched with $LiFePO_4$ particle size and good contact between particles and PPy will be established. Also, the electrolyte can penetrate easily into the electrode, and hence the rate ability and flexibility of the $LiFePO_4$ have been enhanced significantly.

2. Experimental

NiTi was deposited onto a flexible glass using ultra-high vacuum DC magnetron sputtering. After making a base vacuum of less than 10^{-6} Pa, the chamber was cooled down using liquid nitrogen. Two separate elemental targets (Ni and Ti) were used with a rotary (10 rpm) substrate holder in argon (5 N) flow. The NiTi-coated samples were used as substrates for polypyrrole synthesizing. PPy was synthesized electrochemically using 0.1 M pyrrole monomer (MERCK, Germany) and 0.1 M $LiClO_4$ in an aqueous solution. The solution was prepared by adding the $LiClO_4$ and then pyrrole monomer with mild stirring. The galvanostatic method was applied at a constant current density of 0.2 mA cm^{-2} using Autolab PGSTAT30 with Pt rod as the counter electrode for electropolymerization. The process of deposition lasts for five minutes in constant current density. For characterization of the PPy film, FTIR spectroscopy was used (Bruker, Vector33).

$LiFePO_4$ was synthesized using a typical high-temperature method using mixed and ball-milled $NH_4H_2PO_4$, Li_2CO_3, and $FeC_2O_4.2\ H_2O$ powders with a stoichiometric ratio in a tube furnace under 5 N nitrogen at 750 °C for 24 h. The morphology of the $LiFePO_4$ powders and electropolymerized PPy was evaluated using scanning electron microscopy (SEM, Philips XL30).

The cathodes were fabricated from a mixture of active material (85 wt%), carbon black (10 wt%), and polyvinylidene fluoride (PVDF) (5 wt %) in N-methyl-2-pyrrolidione (NMP) solvent. For the pure $LiFePO_4$ cathode, the slurry was cast onto the NiTi-coated flexible glass. For the $LiFePO_4$/PPy cathode, the slurry was cast after the electrodeposition of the PPy on the NiTi-coated flexible glass. After evaporating the solvent in a vacuum oven, the electrode was pressed. Lithium metal was employed as the counter electrode. The electrolyte was prepared by using 1 M $LiPF_6$ in a 50:50 (v/v) mixture of ethylene carbonate (EC) and dimethyl carbonate (DMC). The 2032 coin cells consisting of the cathode, lithium, and electrolyte were assembled in the glove box (in Ar atmosphere). Charging and discharging of the cells were done galvanostatically in the 2.5–4.0 V range at a constant current density of 0.1 mA cm^{-2}. Cyclic voltammetry experiments were done at a scanning rate of 0.1 mV/s using an Autolab PGSTAT30.

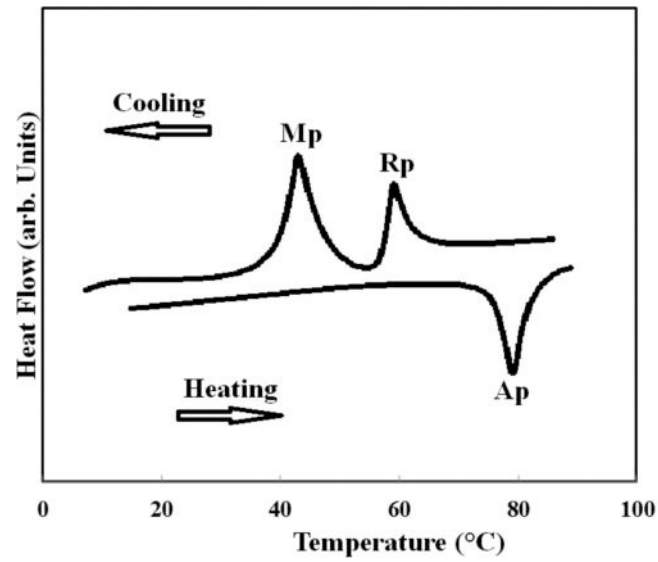

Fig. 2. The DSC plot of the sputtered NiTi thin film on the flexible glass.

3. Results and discussion

Fig. 1 represents the SEM images of the NiTi surface and cross-section. The surface morphology of the NiTi thin film consists of a uniform and fine structure. The thickness of the sputtered film is 61.67 nm. The uniform and 2D structure of the coating confirmed the Frank-van der Merwe (FvdM) growth mode of NiTi thin film growth by DC sputtering.

The DSC plot in Fig. 2 represents the phase transformation of the NiTi thin film. An endothermic and two exothermic peaks are observed in the heating and cooling curves due to the presence of the *R* phase. The downward endothermic peak (Ap) is associated with austenitic transformation from 72 °C to 84 °C. In the cooling plot, the upward peak of Rp represents the transformation of the austenite phase to the rhombohedral *R*-phase, followed by the Mp peak related to the martensite phase.

Cyclic voltammetry was employed to investigate the electrodeposition process of the pyrrole on the NiTi layer. Fig. 3(a) shows the voltammograms of electropolymerization of the pyrrole in the presence of $LiClO_4$ and Na_2SO_4. The oxidation peak relating to the Py monomer started at + 0.85 V (vs. Ag/AgCl) in $LiClO_4$. In contrast, the electropolymerization peak in the presence of Na_2SO_4 occurred at a lower potential, + 0.65 V. The current density was increased by decreasing the potential, showing better monomer oxidation on freshly electropolymerized PPy. During electrodeposition, ClO_4^- doped into the polymeric chain [22]:

$$[Py]_n + nqClO_4^- \xrightarrow{doping} \left[Py^{q+}\left(ClO_4^-\right)_q\right]_n + nqe^-$$

The voltammograms revealed a higher polymerization rate for Na_2SO_4 than $LiClO_4$. At a potential of 1.1 V, the current density for Na_2SO_4 and $LiClO_4$ is 6.75 μA/cm^2 and 0.75 μA/cm^2.

The working electrode was made by deposition of PPy at a constant

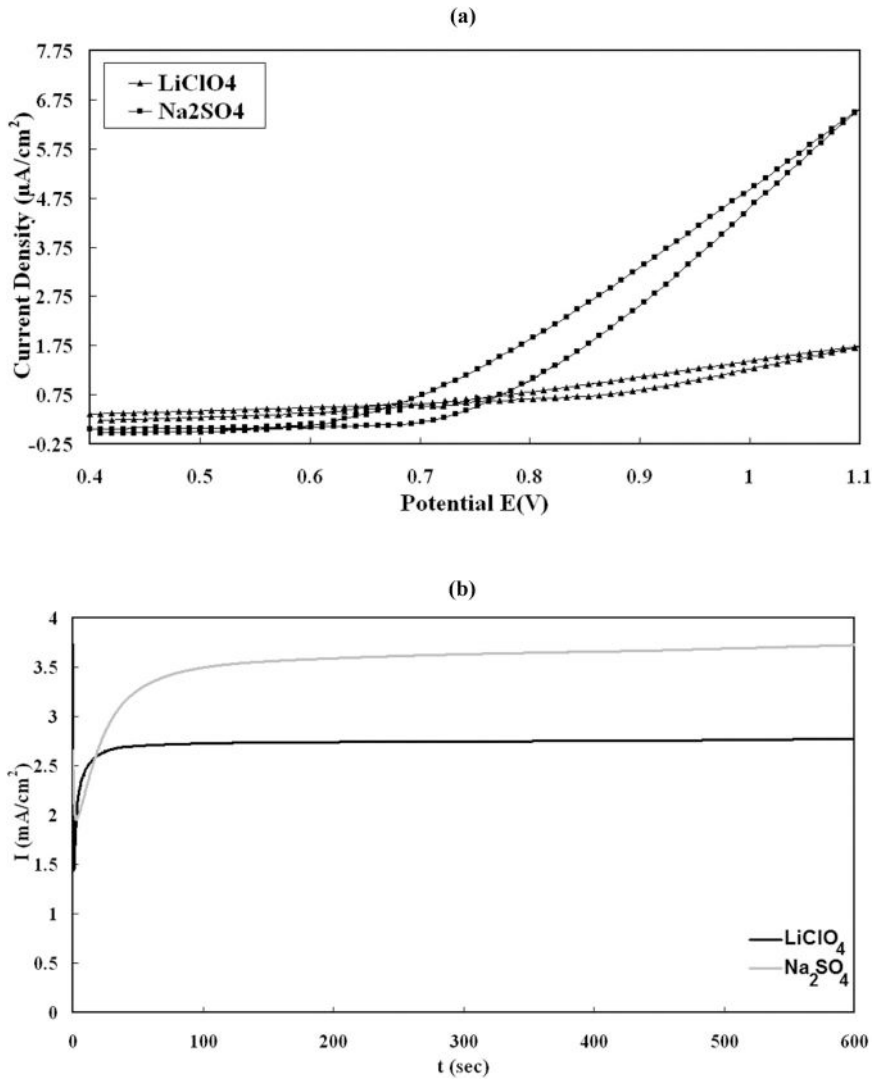

Fig. 3. (a) Cyclic voltammograms of microfibrillar PPy deposition on the NiTi ($\nu = 20$ mV/s) and (b) Potentiostatic I–t transients for electropolymerization of the microfibrillar PPy on NiTi at E = +0.9 V versus Ag/AgCl in the presence of $LiClO_4$ and Na_2SO_4.

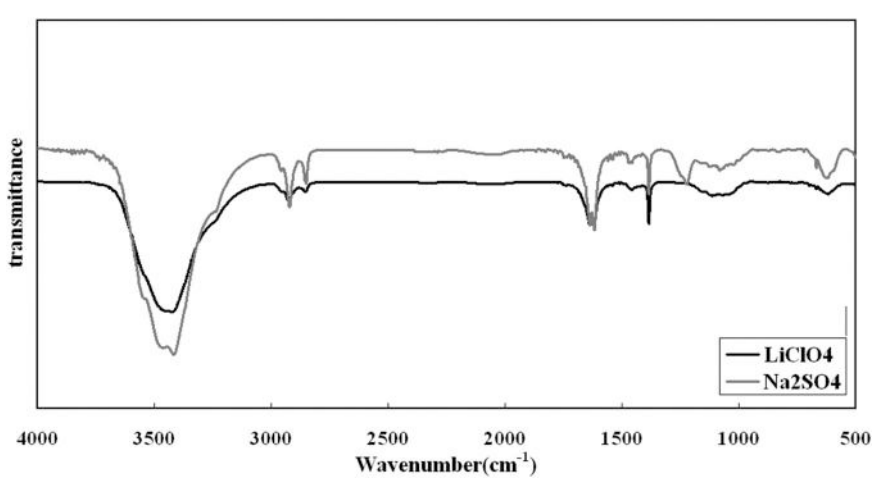

Fig. 4. FTIR spectra of the electrodeposited microfibrillar PPy in the solutions containing $LiClO_4$ and Na_2SO_4.

voltage of + 0.9 V. The lower potential leads to minimizing the side reactions. Fig. 3(b) shows the I-t transient for deposition of the PPy film. The electropolymerization current was increased due to the formation of new PPy film onto the electrode. The higher current density is observed for Na_2SO_4, which emphasizes a higher polymerization rate of the Py.

Fig. 4 shows the FTIR spectrum of the PPy films. The prominent

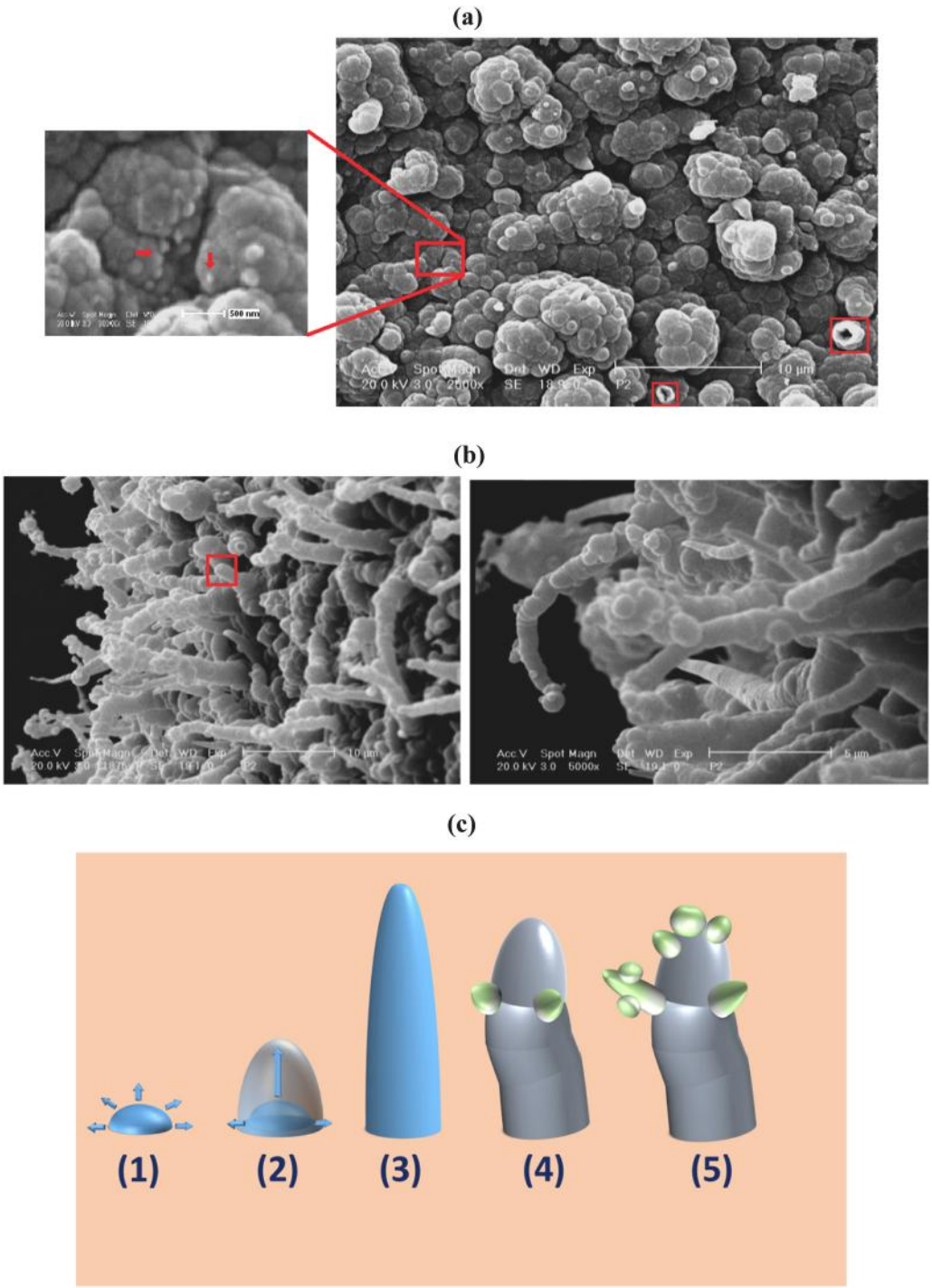

Fig. 5. (a, b) SEM images of the microfibrillar PPy film at the top and tilted views and (c) a schematic of the growth mechanism of the microfibrils.

peaks involve 3400 [-NH], 2920 [-CH: in —CH_3], 1600 [C=C/C—C], 1380 [—CN], 1100 [—CH: plane], and 660 [—CH: rocking]. The vast and strong absorption band at around 3410–3460 cm^{-1} is related to the N–H stretching. The 2750–3000 cm^{-1} peaks correspond to the aromatic C–H stretching vibrations in the –CH_3 group due to the dopant or its dislocation effect among the polymer chain layers. The band at 1600 cm^{-1} is due to the stretching vibrations of the C=C/C–C. The 1100–1250 cm^{-1} band is related to the breathing vibrations of the pyrrole ring, C–C out-of-plane ring deformation, or C–H rocking. From the above results, it can be concluded that polypyrrole films were successfully formed under the electrochemical conditions used in this work.

The morphology of the PPy film was examined using SEM (Fig. 5(a-c)). Fig. 5(a) shows the morphology of the PPy film from the top view, consisting of a globular structure with a cauliflower view. The difference in the height of the polypyrrole deposits is seen as a contrast in the SEM images. During PPy electrodeposition, some tubular structures were also formed, as indicated in Fig. 5(a). A fine structure is observed at higher magnification, and white globular PPy was formed during electropolymerization, which is indicated by arrows. These deposits have sizes less than 100 nm and were grown at various points of the surface. The successive layers of the PPy film were formed from these nuclei.

By tilting the sample, the microfibrillar morphology of the deposited PPy was observed (Fig. 5(b)). The fibril length is in the range of 5–10 μm. Almost all of the fibrils were grown aligned and perpendicular

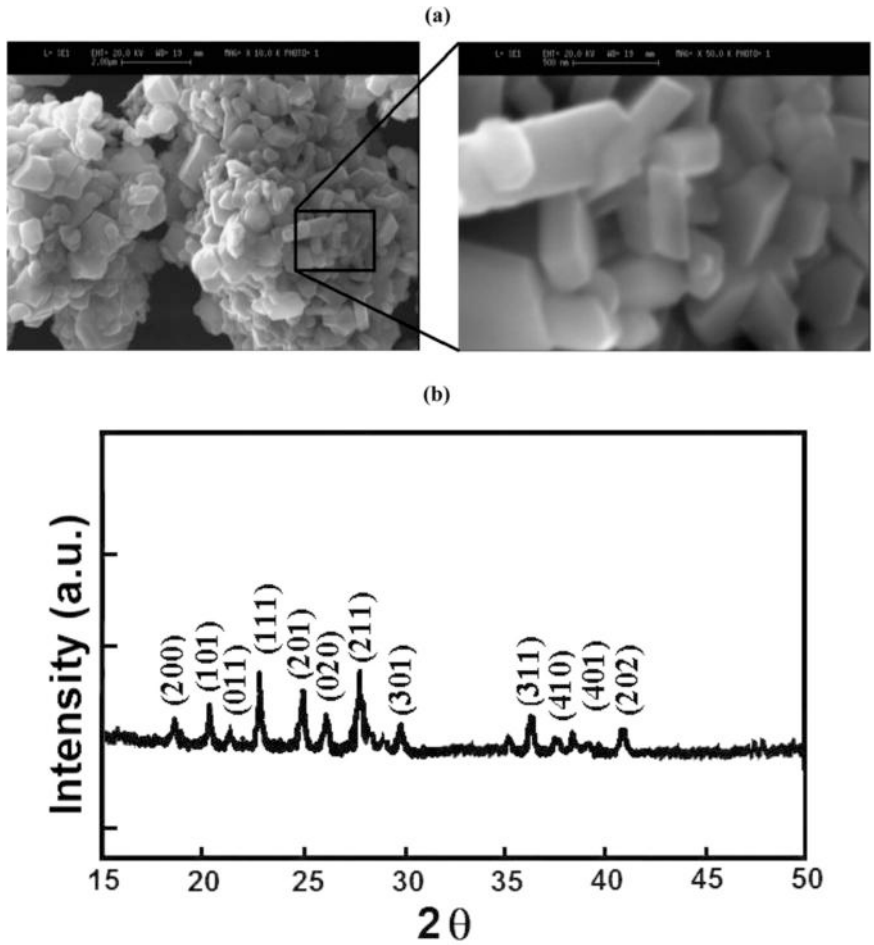

Fig. 6. (a) SEM images in different magnifications and (b) XRD pattern of the synthesized $LiFePO_4$ powder.

to the surface of the electrode. Tubular deposit is also observed. Various synthesis procedures were employed to fabricate conducting polymers while controlling in size and morphology. These structures consisted of nanowire polyaniline (PANI) [23], tube junctions and dendrites PANI [24], PPy microcontainer [25], Whelk-like Helixes of PPy [26], PPy micro/nanowires [27], PPy hollow spheres [28] and PPy double-shelled hollow particles [29]. Almost all of them applied hard or soft templating to control the morphology and size of the conducting polymers. Surfactants, the major part of the soft-templating process, include sodium dodecyl sulfate (SDS) and Cetyltrimethyl ammonium bromide (CTAB) [30,31]. When the template-free process is considered, the polymerization conditions and media change. For example, in electropolymerization, hydrogen bubbling is introduced into the electrolyte by applying higher working potentials or higher pH [25,32]. So, this is the first report about the formation of the PPy well-defined structure in a typical electropolymerization condition of the pyrrole without any modification of the electrolyte composition, pH, electropolymerization method, and the other effective parameters.

For whelk-like PPy helixes, the globular structure was observed underneath the whelk-like PPy layer [26]. Also, the layer consisted of some conical PPy deposits with or without holes and a trace of the semi-spherical nucleus growing on its surface. The growth mechanism was suggested based on combining two phenomena [26]: First, the diffusing of pyrrole monomers to the interface of the PPy and glassy carbon (GC) electrode followed by polymerizing and pushing away the PPy [33], and second, the electrostatic repulsion of the SDS heads which formed bilayer micelle.

Interestingly, in this study, the dimension of the PPy fibrils base is in the range of 1–3 μm (Fig. 4(b)), which is very close to the whelk-like PPy [26]. Here, the same conic shapes are also observed, and some fibrils have smoother surfaces than others. The nucleation and growth are very clear in the SEM images.

The schematic of the proposed mechanism for nucleation and growth of the PPy fibrils is presented in Fig. 5(c). A nucleus was formed and grown on the surface of the electrode via typical electrochemical nucleation and 3D growth process (step 1). After growing and reaching a critical radius, the growth mechanism changed from 3D to 1D (Step 2), forming conical PPy. The 1D electropolymerization extends the PPy through wire, tube, and fibril. This process was accompanied by increasing the fibril thickness until some nuclei subsequently nucleated and grew on the surface of the PPy fibril (steps 3 and 4), and subsequent growth led to branch off (step 5). Finally, the 3D growth again continued until overlapping of the fibrils and forming a new layer of fibrils.

Naoi et al. presented a mechanism for columnar growth of the PPy in the presence of the SDS. They showed that after a charge density of 60 mC cm^{-2}, a columnar structure was formed. At this point, the height of the grains was less than 100 nm, which was increased at higher charge densities [34]. The same behavior was reported for PPy and $LiClO_4$ in acetonitrile. A transition from 3D nucleation and 1D growth was seen after nuclei overlapped at around 60 mC cm^{-2} and a film thickness of 100 nm [35,36]. We have also seen this transition for the same electrolyte composition in deionized water [21]. However, introducing nanoparticles into the media prevented the change in growth mechanism to 1D.

Conclusively, what makes different morphology of the PPy includes not only the electrolyte composition and solvent [26] but also all electrochemical parameters and the electrodeposition time or charge.

SEM images in Fig. 6(a) show the hexagonal morphology of the

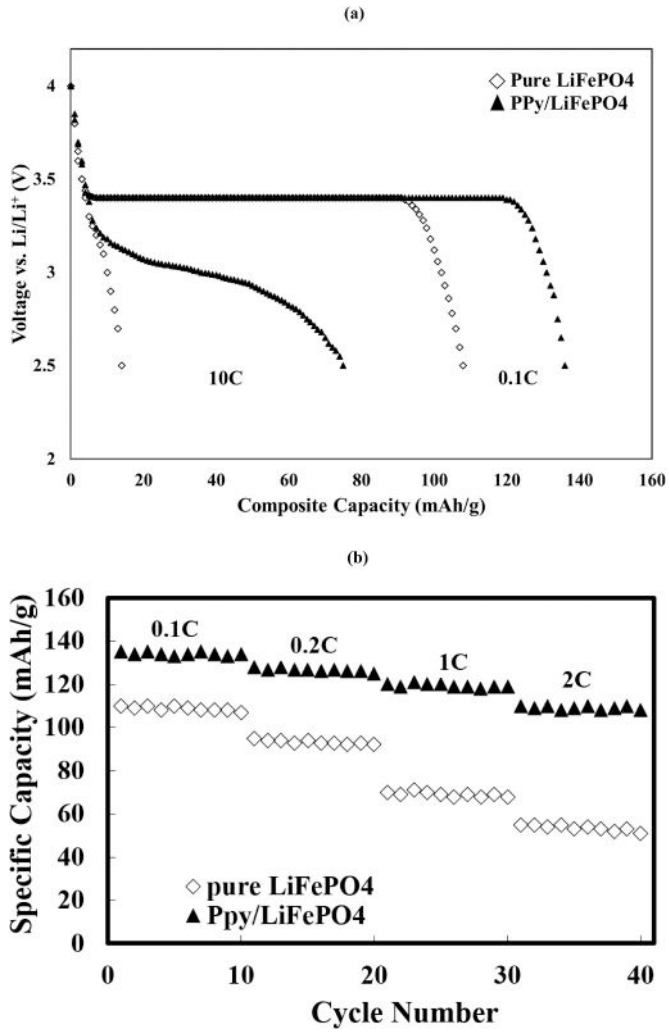

Fig. 7. (a) Discharge curves of pure $LiFePO_4$ and microfibrillar PPy/$LiFePO_4$ cathodes at 0.1–10 C and (b) Rate capabilities of the Pure $LiFePO_4$ and microfibrillar PPy/$LiFePO_4$ cathodes at rates of C/10, C/5, 1 C, and 2 C.

particles with sizes of about 0.5–2 μm for the $LiFePO_4$ powder. The process protocol was designed and controlled for producing particles that apply to the size of the voids in the PPy microfibrils (Fig. 5).

Fig. 6(b) represents the XRD pattern of the $LiFePO_4$ powders. The sample is pure without impurity phases, demonstrating the single-phase orthorhombic olivine with the *Pnma* space group. The crystallite size of the powders was obtained at 156 nm using Scherrer formula $\beta \cos\theta = k\lambda/D$, where β is the full width at half maximum intensity of the peak (FWHM), θ is Bragg's diffraction angle, k is a constant (~0.9), λ is the wavelength of Cu Kα (λ = 1.5405 Å), and D is the mean crystallite size.

Fig. 7(a) shows the discharge plots for pure $LiFePO_4$ and $LiFePO_4$/PPy composite at 0.1–10 C. Before every discharge, the cells were charged at a constant 0.1 C. Each voltage profile shows a plateau at about 3.4 V regarding Fe^{2+}/Fe^{3+} redox. Lower cell polarization is accompanied by a higher discharging voltage plateau for $LiFePO_4$ composite. At 0.1 C, the specific capacities of the pure and composite $LiFePO_4$ are 108 mAh/g and 136 mAh/g, respectively. At a higher discharge rate of about 10 C, almost all of the capacity of the pure $LiFePO_4$ was diminished and reached 15 mAh/g with a discharging voltage of around 3.0 V. The discharging voltage plateau for $LiFePO_4$/PPy is about 3.2 V with a reversible capacity of 75 mAh/g.

Fig. 7(b) shows the cyclability of the pure $LiFePO_4$ and $LiFePO_4$/PPy composite at various rates. At a low discharge rate (C/10), the specific capacity of $LiFePO_4$ reached 110 mAh/g, while $LiFePO_4$/PPy is 137 mAh/g with less fading rate up to 10 cycles. Increasing the discharging rate reduced the reversible specific capacity of both $LiFePO_4$ and its composite with PPy. The effect of PPy microfibrils on the electrochemical performance of the $LiFePO_4$ is most evident at a rate of 2 C, in which the specific capacity of the composite is 50 mAh/g higher than pure $LiFePO_4$. The fading rate of the composite also revealed a more stable performance than pure $LiFePO_4$. The specific capacity of the $LiFePO_4$ is less than 50 mAh/g, while its composite is still higher than 100 mAh/g after ten cycles in 2 C.

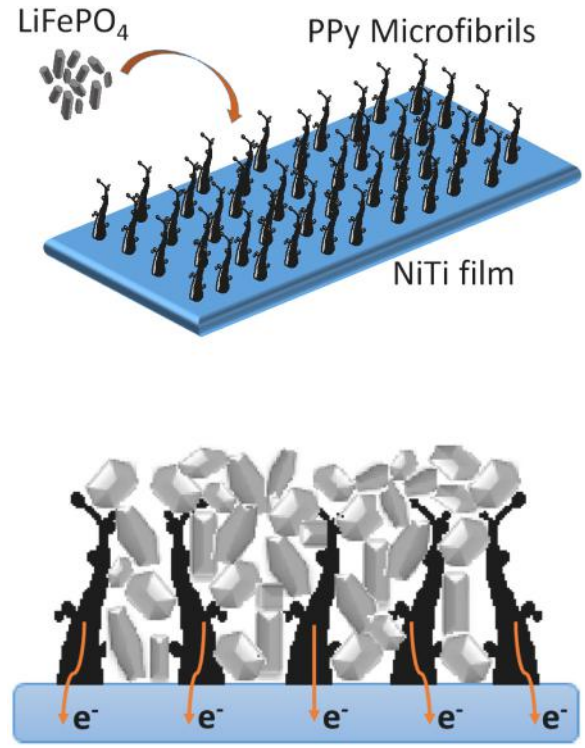

Fig. 8. Schematic of the composite cathode electrode's electron and ion transfer pathways via PPy microfibrils.

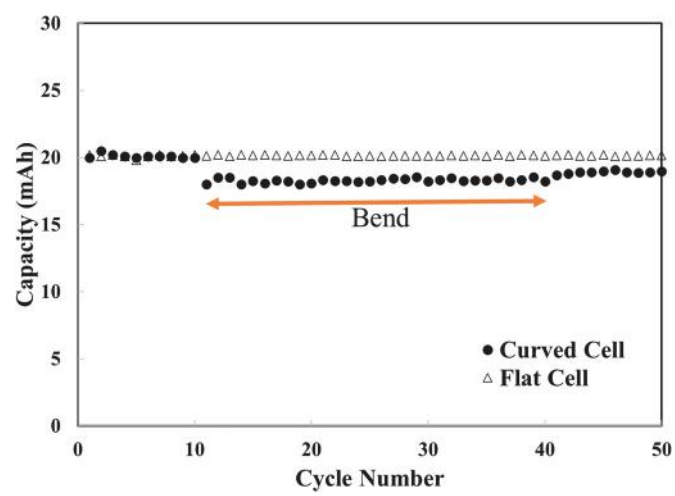

Fig. 9. Cyclic performance of the bent single-layer pouch cell with $LiFePO_4$/PPy cathode on NiTi at 1 C.

Fig. 8 demonstrated that the PPy microfibrils behave as electrical pathways for faster electron and ion transfer for $LiFePO_4$ with low electrical conductivity. This mechanism also led to lower polarization

Table 1
Comparison of the present study results with the literature.

Cathode	Flexible	Preparation method	Capacity-mAh (C-rate)	Cyclic performance-mAh (cycle No., C-rate)	Voltage Window (V)	Ref.
$LiFePO_4$/PPy	No	Electrodeposition	110–132 (0.2 C)	132 (10, 0.2 C)	2.5–4.1	[9]
$LiFePO_4$/PPy	No	Chemical oxidation	144.5 (0.1 C)	135 (10, 0.1 C)	2.5–4.3	[11]
$LiFePO_4$/PPy	No	Chemical oxidation	153 (0.1 C)	150 (100, 0.1 C)	2.5–4.0	[12]
$LiFePO_4$/C-PPy	No	Chemical vapor deposition	~147 (1 C) 80 (20 C)	-	2.0–4.2	[13]
$LiFePO_4$/PPy	No	Vapor-phase polymerization	106.7 (10 C)	91.2 (500, 10 C)	2.5–3.9	[14]
$LiFePO_4$-PPy(25%)/C	No	In-situ pulverization	209.1 (0.1 C) 86.1(10 C)	137.5 (500, 0.5 C)	2.0–4.0	[15]
$LiFePO_4$/PPy	No	In-situ chemical oxidation	160 (0.1 C) 92 (20 C)	143 (500, 1 C)	2.5–4.2	[16]
$LiFePO_4$/PPy	Yes	Electrodeposition	136 (0.1 C) 75 (10 C)	137 (10, 0.1 C) 105 (10, 2 C)	2.5–4.0	This Work

and, consequently, higher plateau voltage at higher C-rates.

Fig. 9 shows the capacity retention of the curved single-layer cell with lithium anode. The cyclic performance of the flat cell is uniform until the 50th cycle, with a capacity of about 20mAh. For the curved cell, the capacity fell from 20mAh to about 18mAh after bending, and this capacity was retained until the 40th cycle when the cell was relieved. Then, the capacity increased again and reached about 19mAh, revealing the appropriate cathode flexibility using PPy microfibrils.

Table 1 compares the results of the current study with the literature [9, 11–16]. As can be seen, the chemical oxidation method is used for embedding the PPy into the cathode since the electrodeposition did not successfully reach a high discharge rate [9]. Applying the carbon in addition to the PPy resulted in a higher capacity of the $LiFePO_4$ [13,15]. However, selecting a wider voltage window also is effective [11,13,15, 16]. None of the mentioned works designed the cathodes for flexible smart devices. This work proposed the flexible cathode based on the nanocomposite of the electrodeposited PPy microfibrils with $LiFePO_4$ on the shape memory NiTi with high capacity in a high discharge rate.

4. Conclusion

Shape memory thin film NiTi was deposited using sputtering with a thickness of 61.67 nm. The DSC test revealed the martensitic transformation at room temperature, which helps the battery flexibility. The PPy microfibrils were electrodeposited with a 5–10 μm length and examined using FTIR. The novel mechanism of 1D growth of these microfibrils was investigated in detail. The electrochemical performance of the synthesized $LiFePO_4$ with the size of 0.5–2 μm showed that applying PPy microfibrils increased the capacity from 108 to 136 mAh/g at 0.1 C and significantly improved rate capability. The half-cell test results revealed a five times higher capacity for microfibril PPy-$LiFePO_4$ nanocomposite concerning pure $LiFePO_4$. The cyclic performance of the curved electrode also showed a little loss (about 1 mAh for a 20 mAh electrode) in capacity with appropriate recovery at 1 C. As all the materials used in this study are biocompatible, such results can introduce a new field in flexible batteries for wearable devices, MEMS, and self-powered bioimplants.

CRediT authorship contribution statement

M. Torabi worked out the technical details and wrote the initial version of the manuscript. S.K. Sadrnezhaad devised the main conceptual idea, proof outline and edited the final version of the paper.

Declaration of Competing Interest

The authors declare that they have no known competing financial interests or personal relationships that could have appeared to influence the work reported in this paper.

Data availability

Data will be made available on request.

References

[1] A.K. Padhi, K.S. Nanjundaswamy, J.B. Goodenough, Phospho-olivines as positive-electrode materials for rechargeable lithium batteries, J. Electrochem. Soc. 144 (1997) 1188–1194, https://doi.org/10.1149/1.1837571.
[2] S.Y. Chung, J.T. Bloking, Y.M. Chiang, Electronically conductive phospho-olivines as lithium storage electrodes, Nat. Mater. 1 (2002) 123–128, https://doi.org/10.1038/nmat732.
[3] N.C.Y. Ravet, J.F. Magnan, S. Besner, M. Gauthier, M. Armand, Electroactivity of natural and synthetic triphylite, J. Power Sources 97–8 (2001) 503–507, https://doi.org/10.1016/S0378-7753(01)00727-3.
[4] P.S. Herle, B. Ellis, N. Coombs, L.F. Nazar, Nano-network electronic conduction in iron and nickel olivine phosphates, Nat. Mater. 3 (2004) 147–152, https://doi.org/10.1038/nmat1063.
[5] M. Torabi, A. Tavakkoli Neyshabouri, B. Soltan Mohammad, S.H. Razavi, M. Kianpour Rad, Effect of milling on the electrochemical properties of nanostructured Li(Fe0.8Mn0.2)PO4 as cathodes for Li-ion batteries, J. N. Mater. Electrochem. Syst. 20 (2017) 39–42, https://doi.org/10.14447/jnmes.v20i1.293.
[6] C. Delacourt, P. Poizot, S. Levasseur, C. Masquelier, Size effects on carbon-free $LiFePO_4$ powders, Electrochem. Solid State Lett. 9 (2006) A352–A355, https://doi.org/10.1149/1.2201987.
[7] D.H. Kim, J. Kim, Synthesis of $LiFePO_4$ nanoparticles in polyol medium and their electrochemical properties, Electrochem. Solid State Lett. 9 (2006) A439–A442, https://doi.org/10.1149/1.2218308.
[8] B. Kang, G. Ceder, Battery materials for ultrafast charging and discharging, Nature 458 (2009) 190–193, https://doi.org/10.1038/nature07853.
[9] K.S. Park, S.B. Schougaard, J.B. Goodenough, Conducting-polymer/iron-redox-couple composite cathodes for lithium secondary batteries, Adv. Mater. 19 (2007) 848–851, https://doi.org/10.1002/adma.200600369.
[10] Y.H. Huang, J.B. Goodenough, High-rate $LiFePO_4$ lithium rechargeable battery promoted by electrochemically active polymers, Chem. Mater. 20 (2008) 7237–7241, https://doi.org/10.1021/cm8012304.
[11] X. Ren, X. Li, P. Zhang, J. Liu, Q. Zhang, Preparation and electrochemical properties of LiFePO4/PPy composite cathode materials for lithium-ion batteries, Adv. Mater. Res. 92 (2010) 155–162, https://doi.org/10.4028/www.scientific.net/AMR.92.155.
[12] A. Fedorková, R. Oriňáková, A. Oriňák, H.D. Wiemhöfer, D. Kaniansky, M. Winter, Surface treatment of LiFePO4 cathode material with PPy/PEG conductive layer, J. Solid State Electrochem 14 (2010) 2173–2178, https://doi.org/10.1007/s10008-009-0967-2.
[13] Q. Gong, Y.S. He, Y. Yang, X.Z. Liao, Z.F. Ma, Synthesis and electrochemical characterization of $LiFePO_4$/C-polypyrrole composite prepared by a simple chemical vapor deposition method, 1388-1388, J. Solid State Electrochem 16 (2012), https://doi.org/10.1007/s10008-011-1538-x.
[14] Q. Xiao, Y. Li, Y. Zhang, S. Huang, Interfacial coupling-induced pseudocapacitance in $LiFePO_4$@polypyrrole heterostructures toward high-rate lithium storage, Energy Technol. 11 (2023) 2300361, https://doi.org/10.1002/ente.202300361.
[15] Z. Chen, Y. Wang, M. Wang, F. Yong, W. Luo, M. Zhao, F. Yu, Synergy and symbiosis analysis of capacity-contributing polypyrrole and carbon-coated lithium iron phosphate nanostructures for high-performance cathode materials, ACS Appl. Nano Mater. 6 (2023) 7465–7476, https://doi.org/10.1021/acsanm.3c00628.
[16] X. Li, F. Jiang, K. Qu, Y. Wang, Y. Pan, M. Wang, Y. Liu, H. Xu, J. Chen, Y. Huang, J. Zheng, P. Gao, M. Chen, J. Li, Y. Peng, D. Mitlin, First atomic - scale insight on degradation in lithium iron phosphate cathodes by transmission electron microscopy, J. Phys. Chem. Lett. 11 (2020) 4608–4617, https://doi.org/10.1021/acs.jpclett.0c00317.
[17] W. Wang, D. Yang, Z. Huang, H. Hu, L. Wang, Kai Wang, Electrodeless nanogenerator for Dust Recover, Energy Technol. 10 (2022) 2200699, https://doi.org/10.1002/ente.202200699.

[18] M. Zhang, W. Wang, G. Xia, L. Wang, K. Wang, Self-powered electronic skin for remote human–machine synchronization, ACS Appl. Electron. Mater. 5 (2023) 498–508, https://doi.org/10.1021/acsaelm.2c01476.
[19] Z. Yi, Z. Chen, K. Yin, L. Wang, K. Wang, Sensing as the key to the safety and sustainability of new energy storage devices, Prot. Control Mod. Power Syst. 8 (2023) 27, https://doi.org/10.1186/s41601-023-00300-2.
[20] M. Zhang, D. Yang, J. Du, H. Sun, L. Li, L. Wang, K. Wang, A Review of SOH prediction of li-ion batteries based on data-driven algorithms, Energies 16 (2023) 3167, https://doi.org/10.3390/en16073167.
[21] M. Torabi, M. Soltani, S.K. Sadrnezhaad, Impedance analysis of growth and morphology of electropolymerized polypyrrole nanocomposites, J. N. Mater. Electrochem. Syst. 17 (2014) 129–132, https://doi.org/10.14447/jnmes.v17i2.434.
[22] Y.H. Huang, K.S. Park, J.B. Goodenough, Improving Lithium Batteries by Tethering Carbon-Coated $LiFePO_4$ to Polypyrrole, J. Electrochem. Soc. 153 (2006) A2282–A2286, https://doi.org/10.1149/1.2360769.
[23] Sh.-J. Choi, S.-M. Park, Electrochemical growth of nanosized conducting polymer wires on gold using molecular templates, Adv. Mater. 12 (2000) 1547–1549, https://doi.org/10.1002/1521-4095(200010)12:20%3C1547::AID-ADMA1547%3E3.0.CO;2-1.
[24] Zh Wei, L. Zhang, M. Yu, Y. Yang, M. Wan, Self-assmbling sub-micrometer-sized tube junctions and dendrites of conducting polymers, Adv. Mater. 15 (2003) 1382–1385, https://doi.org/10.1002/adma.200305048.
[25] L. Qu, G. Shi, F. Chen, J. Zhang, Electrochemical growth of polypyrrole microcontainers, Macromolecules 36 (2003) 1063–1067, https://doi.org/10.1021/ma021177b.
[26] G. Chen, Zh Wang, D. Xia, L. Zhang, R. Hui, J. Zhang, Whelk-like helixes of polypyrrole synthesized by electropolymerization, Adv. Func. Mater. 17 (2007) 1844–1848, https://doi.org/10.1002/adfm.200600828.
[27] G. Lu, C. Li, G. Shi, Polypyrrole micro- and nanowires synthesized by electrochemical polymerization of pyrrole in the aqueous solutions of pyrenesulfonic acid, Polymer 47 (2006) 1778–1784, https://doi.org/10.1016/j.polymer.2006.01.081.
[28] D. Su, J. Zhang, Sh. Dou, G. Wang, Polypyrrole hollow nanospheres: Stable cathode materials for sodium-ion batteries, Chem. Commun. 51 (2015) 16092–16095, https://doi.org/10.1039/C5CC04229A.
[29] M.Y. Bai, Y. Xia, Facile synthesis of double-shelled polypyrrole hollow particles with a structure similar to that of a thermal bottle, Macromol. Rapid Comm. 31 (2010) 1863–1868, https://doi.org/10.1002/marc.201000385.
[30] I. Rawal, A. Kaur, Effect of anionic surfactant concentration on the variable range hopping conduction in polypyrrole nanoparticles, J. Appl. Phys. 115 (2014), 043717, https://doi.org/10.1063/1.4863179.
[31] N.D. Gupta, D. Banerjee, N.S. Das, K.K. Chattopadhyay, Kinetics of micelle formation and their effect on the optical and structural properties of polypyrrole nanoparticles, Colloid Surf. A 385 (2011) 55–62, https://doi.org/10.1016/j.colsurfa.2011.05.044.
[32] K.P. Díaz-Orellana, M.E. Roberts, Scalable, template-free synthesis of conducting polymer microtubes, RSC Adv. 5 (2015) 25504–25512, https://doi.org/10.1039/C4RA16000B.
[33] Ch Jérôme, R. Jérôme, Electrochemical Synthesis of Polypyrrole Nanowires, Angew. Chem. Int. Ed. 37 (1998) 2488–2490, https://doi.org/10.1016/j.elecom.2019.04.007.
[34] K. Naoi, Y. Oura, M. Maeda, S. Nakamura, Electrochemistry of Surfactant-Doped Polypyrrole Film (I): Formation of Columnar Structure by Electropolymerization, J. Electrochem. Soc. 142 (1995) 417–420, https://doi.org/10.1149/1.2044042.
[35] G. Garcia-Belmonte, J. Bisquert, Impedance analysis of galvanostatically synthesized polypyrrole films. Correlation of ionic diffusion and capacitance parameters with the electrode morphology, Electrochim. Acta 47 (2002) 4263–4272, https://doi.org/10.1016/S0013-4686(02)00510-8.
[36] G. Garcia-Belmonte, Effect of electrode morphology on the diffusion length of the doping process of electronically conducting polypyrrole films, Electrochem. Commun. 5 (2003) 236–240, https://doi.org/10.1016/S1388-2481(03)00037-7.